







Article

Preparation of Pd–Ni Nanoparticles Supported on Activated Carbon for Efficient Removal of Basic Blue 3 from Water

Sultan Alam ¹, Muhammad Sufaid Khan ¹ , Ali Umar ¹, Rozina Khattak ², Najeeb ur Rahman ¹, Ivar Zekker ^{3,*}, Juris Burlakovs ⁴ , Sergio S. dC Rubin ^{5,6} , Makarand Madhao Ghangrekar ⁷ , Gourav Dhar Bhowmick ⁷, Anna Kallistova ⁸, Nikolai Pimenov ⁸, Abbas Khan ⁹  and Muhammad Zahoor ^{10,*} 

¹ Department of Chemistry, University of Malakand, Chakdara 18800, Pakistan; dr.sultanalam@yahoo.com (S.A.); sufaidkhan1984@gmail.com (M.S.K.); aliumar3937@gmail.com (A.U.); rnrnajeab@yahoo.com (N.u.R.)

² Department of Chemistry, Shaheed Benazir Bhutto Women University, Peshawar 25000, Pakistan; rzkhattak@yahoo.com

³ Faculty of Science, Institute of Chemistry, University of Tartu, 14 Ravila St., 50411 Tartu, Estonia

⁴ Department of Water Management, Estonian University of Life Sciences, 5 Kreutzwaldi St., 51014 Tartu, Estonia; Juris.burlakovs@emu.ee

⁵ Georges Lamaitre Center for Earth and Climate Research, Earth and Life Institute, Université Catholique de Louvain, B-1348 Louvain, Belgium; sergio.rubin@uclouvain.be

⁶ Centro Nacional de Investigaciones Biotecnológicas (CNIB), 429 Cala Cala, Cochabamba 2500, Bolivia

⁷ Department of Agricultural and Food Engineering, Indian Institute of Technology Kharagpur, Kharagpur 721302, India; ghangrekar@civil.iitkgp.ernet.in (M.M.G.); gourav.db@gmail.com (G.D.B.)

⁸ Research Centre of Biotechnology of the Russian Academy of Sciences, Winogradsky Institute of Microbiology, Leninsky Prospect, 33, Build. 2, 119071 Moscow, Russia; kallistoanna@mail.ru (A.K.); npimenov@mail.ru (N.P.)

⁹ Department of Chemistry, Abdul Wali Khan University, Mardan 23200, Pakistan; abbas053@gmail.com

¹⁰ Department of Biochemistry, University of Malakand, Chakdara 18800, Pakistan

* Correspondence: ivar.zekker@ut.ee (I.Z.); mohammadzahoorus@yahoo.com (M.Z.)



Citation: Alam, S.; Khan, M.S.; Umar, A.; Khattak, R.; Rahman, N.u.; Zekker, I.; Burlakovs, J.; Rubin, S.S.d.; Ghangrekar, M.M.; Bhowmick, G.D.; et al. Preparation of Pd–Ni Nanoparticles Supported on Activated Carbon for Efficient Removal of Basic Blue 3 from Water. *Water* **2021**, *13*, 1211. <https://doi.org/10.3390/w13091211>

Academic Editor: Zacharias Frontistis

Received: 1 April 2021

Accepted: 25 April 2021

Published: 27 April 2021

Publisher's Note: MDPI stays neutral with regard to jurisdictional claims in published maps and institutional affiliations.



Copyright: © 2021 by the authors. Licensee MDPI, Basel, Switzerland. This article is an open access article distributed under the terms and conditions of the Creative Commons Attribution (CC BY) license (<https://creativecommons.org/licenses/by/4.0/>).

Abstract: Pd–Ni nanoparticles supported on activated carbon (Pd–Ni/AC) were prepared using a phase transfer method. The purpose of synthesizing ternary composites was to enhance the surface area of synthesized Pd–Ni nanoparticles, as they have a low surface area. The resulting composite was characterized by scanning electronic microscopy (SEM), X-ray diffraction (XRD) and energy-dispersive X-ray spectroscopy (EDX) for investigating its surface morphology, particle size, percentage of crystallinity and elemental composition, respectively. The XRD data and EDX analysis revealed the presence of Pd–Ni alloys impregnated on the AC. Pd–Ni/AC was used as an adsorbent for the removal of the azo dye basic blue 3 from an aqueous medium. Kinetic and isotherm models were used to calculate the adsorption parameters. The most suitable kinetic model amongst the applied models was the pseudo-second-order model, confirming the chemisorption characteristics of the process, and the most suitable isotherm model was the Langmuir model, with a maximum adsorption capacity of 333 mg/g at 333 K. Different experimental parameters, such as the adsorbent dosage, pH, temperature and contact time, were optimized. The optimum parameters reached were: a pH of 12, temperature of 333 K, adsorbent dosage of 0.01 g and optimum contact time of 30 min. Moreover, the thermodynamics parameters of adsorption, such as Gibbs free energy (ΔG°), enthalpy (ΔH°) and entropy (ΔS°), showed the adsorption processes being exothermic with values of ΔH° equal to -6.206 kJ/mol and being spontaneous with ΔG° values of -13.297 , -13.780 and -14.264 kJ/mol, respectively at 293, 313 and 333 K. An increase in entropy change (ΔS°) with a value of 0.0242 kJ/mol K, indicated the enhanced disorder at a solid–solution interface during the adsorption process. Recycling the adsorbent for six cycles with sodium hydroxide and ethanol showed a decline in the efficiency of the selected azo dye basic blue 3 up to 79%. The prepared ternary composite was found effective in the removal of the selected dye. The removal of other pollutants represents one of the possible future uses of the prepared adsorbent, but further experiments are required.

Keywords: adsorption; parameters; kinetics models; nanoparticles; characterizations; basic blue 3

1. Introduction

Despite the rapid development in water reclamation technologies, water pollution is still a major global problem [1]. Bodies of water have been polluted with harmful chemicals due to rapid industrialization, leading to potable water scarcity [2]. Many pollutants, such as heavy metals, radionuclides, phenols, pesticides, herbicides, antibiotics, dyes, etc. [2–9], are constantly released from industry into the environment. Amongst the mentioned pollutants, dyes are the most hazardous, containing complex unsaturated organic compounds absorbing light in the visible region, thus limiting photosynthesis in aquatic environments [10,11]. Synthetic dyes are widely used in the clothing, paper, leather, oil, pharmaceutical and food industries as coloring agents [12]. In the textile industry, over 10,000 tons of dye are used per year, and about 10–15% of these dyes are in the form of dye residues being released into bodies of water [13]. According to a World Health Organization report, dye contributes about 17–20% to different pollution sources, and of this percentage, 10–15% are azo dyes, which, along with other hazardous effects (carcinogenic), have caused hepatotoxicity in animal testing [2–9].

The discharge of colour products into bodies of water adversely affects the aquatic environment due to their non-biodegradable complex molecular structures and their byproducts, especially in azo dyes [14]. Colour byproducts in wastewater effluents can cause toxicity depending on their exposure period and the dye concentration. Dyes absorb and reflect sunlight entering the water and can thus interfere with bacterial growth and inhibit photosynthesis in aquatic plants [15,16]. The toxicity of dyes may occur either due to the direct action of the original compound or through its intermediate metabolites, such as naphthalene, benzidine and other aromatic amines. These compounds are byproducts of micro-organisms, and the azo dyes' metabolites are also carcinogenic and mutagenic [17–19]. In human beings, these compounds can cause allergic dermatosis, respiratory diseases, contact dermatitis, asthma, changes in immunoglobulin level and colon and rectum cancer [20–24]. These secondary metabolites can also cause severe genotoxic and phytotoxic effects in plants [25].

Several biological, chemical and physical techniques—such as bacterial, fungal, algal and enzymatic decolorization [26]; phytoremediation; photocatalytic degradation; ozonation; electrolysis; ion exchange; advanced oxidation; membrane filtration; coagulation; flocculation; sonication and adsorption processes—have been used to treat dyes present in wastewater effluents [27–40]. These methods have their own merits, but in terms of versatility and cost, the adsorption process has been found to be superior to other techniques [41–44]. Different adsorbents have been recommended for adsorption of dyes, such as modified alumina, activated clay, activated carbon, kaolinite, bentonite, modified saw dust, fly ash, mesoporous zeolite, metal–organic framework, hydrogels, molecularly imprinted polymer (MIP), metal oxide nanoparticles (NPs), monometallic NPs and bimetallic NPs [45–58].

NPs range in size from 1 to 100 nm, which differs from the bulk material due to their particle size [59]. NPs are widely used in various fields, such as cosmetics, electronics, catalysis, medicine, chemotherapy and water treatment [60–64]. In wastewater treatment, NPs have been used for the removal of pesticides, organic dyes and heavy metals and for the degradation of complex organic pollutants. Various monometallic and bimetallic NPs, such as Pt, Au, Cu, Fe–Ni, Cu–Ag, Fe–Zn, Mn–Zn and Pd–Fe, have been used for the adsorption of dyes [65–72].

Bimetallic nanoparticles (BNPs) that are composed of two different metals, as opposed to monometallic NPs, have drawn the attention of scientists [73]. Comparatively, bimetallic NPs have a large surface area, thus serving as effective catalysts compared with monometallic nanoparticles [74]. Their properties can be further improved to a great extent

when these bimetallic nanoparticles are loaded on a high surface area material, such as activated carbon, graphene oxide, etc. [61].

In this paper, we have synthesized bimetallic Pd–Ni nanoparticles by a phase transfer method; NPs were then impregnated on activated carbon to enhance the surface area of the overall ternary complex. The morphology (shape and size), elemental composition and percentage of crystallinity were analyzed through different instrumental techniques. The supported bimetallic NPs were used for adsorption of basic blue 3 dye from an aqueous medium. The mechanisms and rate of the adsorption process were investigated by applying different kinetic and isotherm models. Furthermore, the adsorbent material used was regenerated by treatment with suitable eluents to check its reproducibility.

2. Materials and Methods

2.1. Chemicals Used

The chemicals used in this study were: palladium (II) chloride (PdCl_2), nickel (II) chloride hexahydrate ($\text{NiCl}_2 \cdot 6\text{H}_2\text{O}$), activated carbon (AC), tetraoctylammonium bromide (TOABr), sodium borohydride (NaBH_4), oleic acid, oleylamine, potassium hydroxide (KOH), sulphuric acid (H_2SO_4), sodium hydroxide (NaOH), toluene, ethanol, acetone, chloroform, 2-propanol, n-hexane and hydrochloric acid (HCl). Basic blue 3 (BB-3) was used as an adsorbate, and its structure is given in Figure 1 while its properties are presented in Table 1. All the chemicals were of analytical grade and were purchased from Sigma-Aldrich (Munich, Germany). The chemicals were used as received without any further purification.

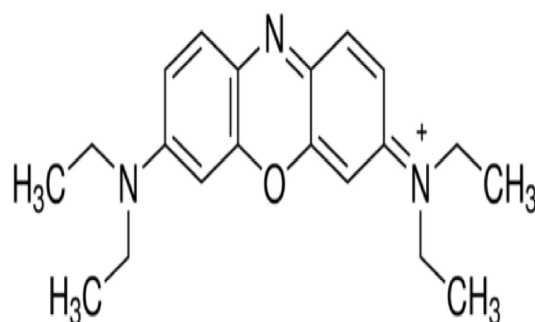


Figure 1. Structure of basic blue 3.

Table 1. Physiochemical properties of basic blue 3.

Name of Dye	Basic Blue 3
Molecular formula	$\text{C}_{20}\text{H}_{26}\text{ClN}_3\text{O}$
Molecular Weight	359.9 g/mol
λ_{max} (Maximum wavelength)	654

2.2. Instrumentation

The synthesized adsorbent was characterized by using a 30 KV scanning electron microscope (JSM5910, JEOL, Tokyo, Japan) with an EDX detector (INCA100/Oxford Instruments, Buckinghamshire, UK), X-ray diffractometer (JDX 3532, JEOL, Tokyo, Japan) with SEI and EDX detectors (INCA200/Oxford Instruments, Buckinghamshire, UK), and a $\text{CuK}\alpha$ source. The dye BB-3 concentration was quantified by measuring absorbance with a double beam UV-vis spectrophotometer (UV-1800, Shimadzu Scientific Instruments Inc., Kyoto, Japan) at a wavelength of 654 nm. The solution pH was determined by using a pH meter. Adsorption tests were conducted in a thermostatic water-bath shaker.

2.3. Synthesis of Supported Bimetallic Palladium-Nickel Nanoparticles

Pd–Ni nanoparticles were synthesized in a two-phase liquid system with slight modification in the reported procedure by adding capping agents, such as oleylamine and oleic

acid [75]. About 5.6 mL of aqueous solution of PdCl₂ (0.022 M) and 5.6 mL of aqueous solution of NiCl₂ (0.033 M) were added to a solution of tetraoctylammonium bromide (TOABr) as a phase-transfer agent in toluene (0.538 g of TOABr in 37 mL of toluene). Then, the solutions were stirred for 2 h. The toluene phase was thereafter separated from the aqueous phase and discarded. The capping agent (23.4 μL of oleic acid and 46 μL of oleylamine) was then added to the mixture and was stirred for another 30 min. To reduce the Pd²⁺ to Pd⁰ and Ni²⁺ to Ni⁰, 35 mL of NaBH₄ solution (0.2 M) was drop wise added into the reaction mixture and stirred for 12 h. After completing the process, the Pd–Ni colloidal particles were obtained, which were then washed with a dilute solution of KOH (5 mM) and distilled water. To support the Pd–Ni particles on the activated carbon, 80 mg of powdered activated carbon was added. After the addition of activated carbon, the mixture was stirred for 12 h. Then, the Pd–Ni powder supported on the activated carbon (Pd–Ni/AC) was separated and purified with chloroform, acetone, toluene and ethanol [75]. The prepared powders were kept in an oven at 70 °C for 2 h and stored in bottles. The summary of the entire procedure is shown in Figure 2.

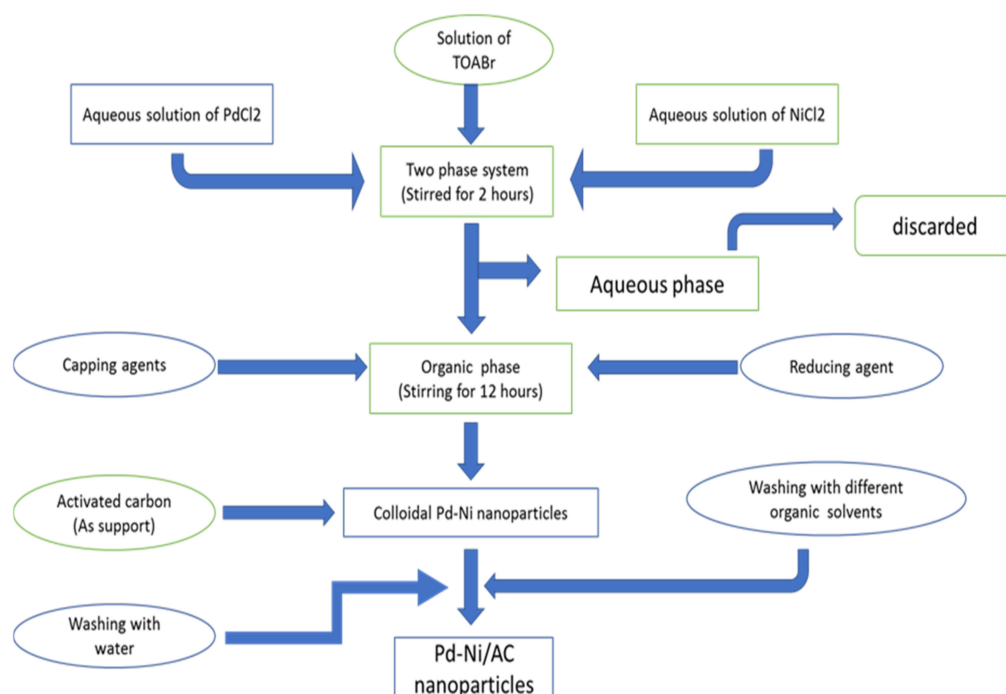


Figure 2. Synthesis of Pd–Ni supported on activated carbon.

2.4. Adsorption Experiments

The adsorption of basic blue 3 dye on the prepared adsorbent was performed at a pH of 12. About 0.01 g Pd–Ni/AC was mixed with a 10 mL solution of BB-3 in reagent bottles. The pH of the solutions was adjusted by the addition of a few drops of HCl (0.1 M) or NaOH (0.1 M) based on the requirement of the experiments. The solutions were mixed in a thermostatic water bath shaker for different time intervals. The reagent bottles were removed from the shaker at a predetermined time, the adsorbent was separated and the concentration of BB-3 dye in the filtrate was measured by a UV-vis spectrophotometer at a wavelength of λ_{\max} 654 nm. The dye's concentration was determined based on the calibration curve drawn for a concentration range. The adsorption capacity of adsorbent q_t (mg g⁻¹) and the removal efficiency were calculated by using Equations (1) and (2), respectively, according to a comparative study performed [76,77]:

$$q_t = \frac{C_0 - C_t}{W} V \quad (1)$$

$$\%R = \frac{C_0 - C_t}{C_0} \times 100 \quad (2)$$

where q_t is the amount of dye adsorbed (mg/g), %R is the percentage of dye removal efficiency, C_0 is the initial concentration of dye (mg/L), C_t is the concentration of dye after adsorption, V is the volume of dye solution (mL) and W is the weight of the adsorbent (g). Various kinetics models were used to enumerate the kinetic constants of adsorption.

Adsorption isotherm experiments were performed on different concentrations, which ranged from 50 mg/L to 500 mg/L with 0.01 g of the prepared adsorbent, while the pH kept was 12. After the addition of the adsorbent, the solutions were stirred for 1 h. Thereafter, the adsorbent was separated from the solution through filtration, and at 654 nm the remaining concentrations were determined using a UV-vis spectrophotometer.

Similar effects of adsorbent dosage, pH and temperature were determined for 100 mg/L solutions, keeping the other parameters the same as the aforementioned.

3. Results and Discussion

3.1. Characterization of Pd–Ni/AC Morphology and Elemental Composition

The surface morphology of Pd–Ni/AC was determined by SEM analysis. The SEM images are given in Figure 3a–d. The micrographs show rough interfaces along with many holes and nanoparticles spreading over the material. Overall, the surface shows irregular particle channels for the adsorption of the specified dye.

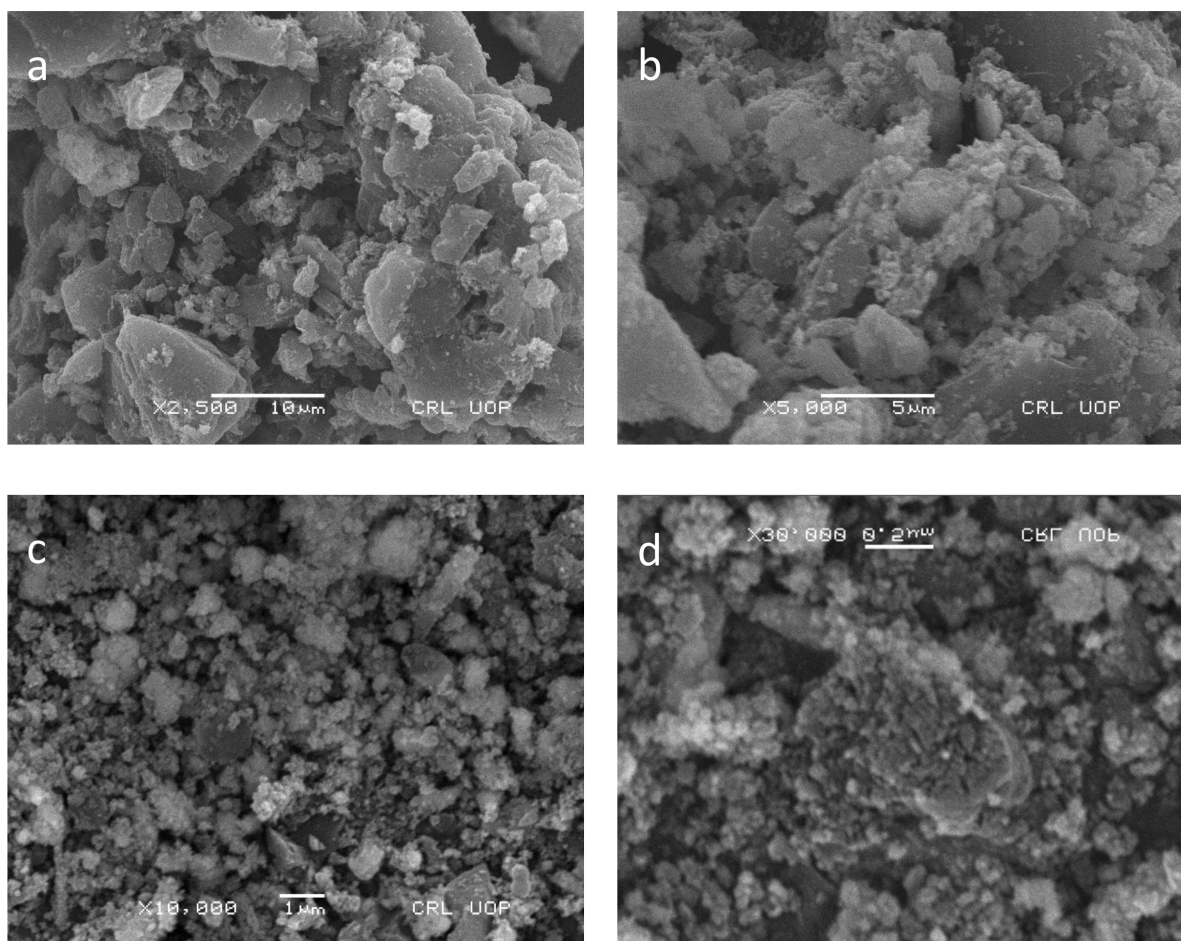


Figure 3. SEM images of Pd–Ni supported on activated carbon at different magnifications of (a) 5000×, (b) 10,000×, (c) 30,000×, (d) 2500×.

Figure 4a shows the EDX elemental analysis of the prepared adsorbent. The results show that elemental atomic weight percentages of Pd–Ni/AC were found to be: C (56.63%), O (13.56%), Pd (29.30%) and Ni (0.51%). Similarly, Figure 4b presents the XRD pattern for the Pd–Ni/AC adsorbent. According to the Scherer formula, the calculated crystallite size is 7.4 nm while the crystallinity is determined to be 83%. Moreover, the characteristic peaks confirm the existence of the Pd–Ni alloy formation.

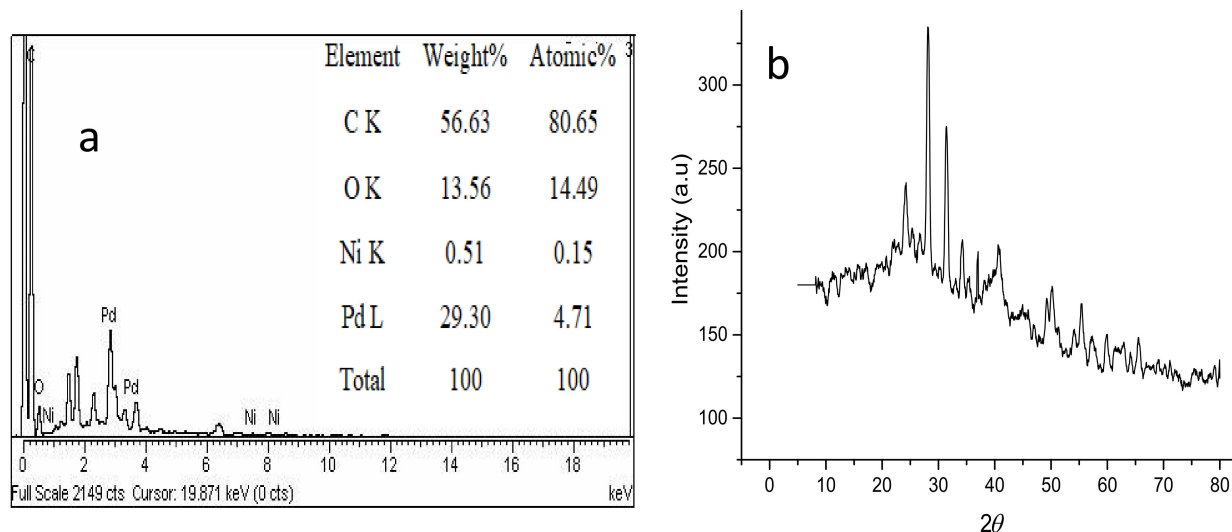


Figure 4. (a) EDX analysis; (b) X-rays Diffraction (XRD) spectrum of the Pd–Ni/AC.

3.2. Adsorbent Dosage Effect on Adsorption

Different adsorbent dosages (0.005–0.03 g) were used to find the optimum amount of adsorbent used for BB-3 removal from the aqueous media in the adsorption experiments. The results are shown in Figure 5a, emphasizing that a linear increase occurred in the removal efficiency of dye with an increase in adsorbent dosage up to 0.01 g of the adsorbent, which was due to the increase of adsorbent surface area and the greater availability of the adsorption active sites. Hence, about 0.01 g of adsorbent dosage was used as the optimal dosage in the subsequent experiments.

3.3. Effect of pH on Adsorption

The acidic or basic media had a major effect on the nature and charge of the adsorbent, as well as on BB-3 adsorption. BB-3 adsorption was investigated at different pH levels (1–14). According to Figure 5b, the maximum dye removal was obtained at pH (8–12). As the dye is cationic in nature, high pH favorability was encountered and optimum adsorption values were achieved. The second most contributing factor was soft–soft interaction between the functional groups that were present at the adsorbate and the metal centers at the adsorbent. At high pH (8–12), electrostatic interaction between the adsorbent and the dye, as well as the dye’s metal center interaction, enhanced the BB-3 removal efficiency. At lower pH, the decrease in the removal efficiency of BB-3 might be due to H⁺ ion competition with BB-3 molecules for the adsorption sites at the adsorbent.

3.4. Effect of Contact Time on Adsorption of BB-3

It was found that the extent of dye removal was improved by increasing contact time, and a maximum value was reached after 30 min. Figure 5c demonstrates that after 30 min contact time, there was no significant effect on dye adsorption observed. Thus, a 30 min reaction time was considered to be the optimum contact time.

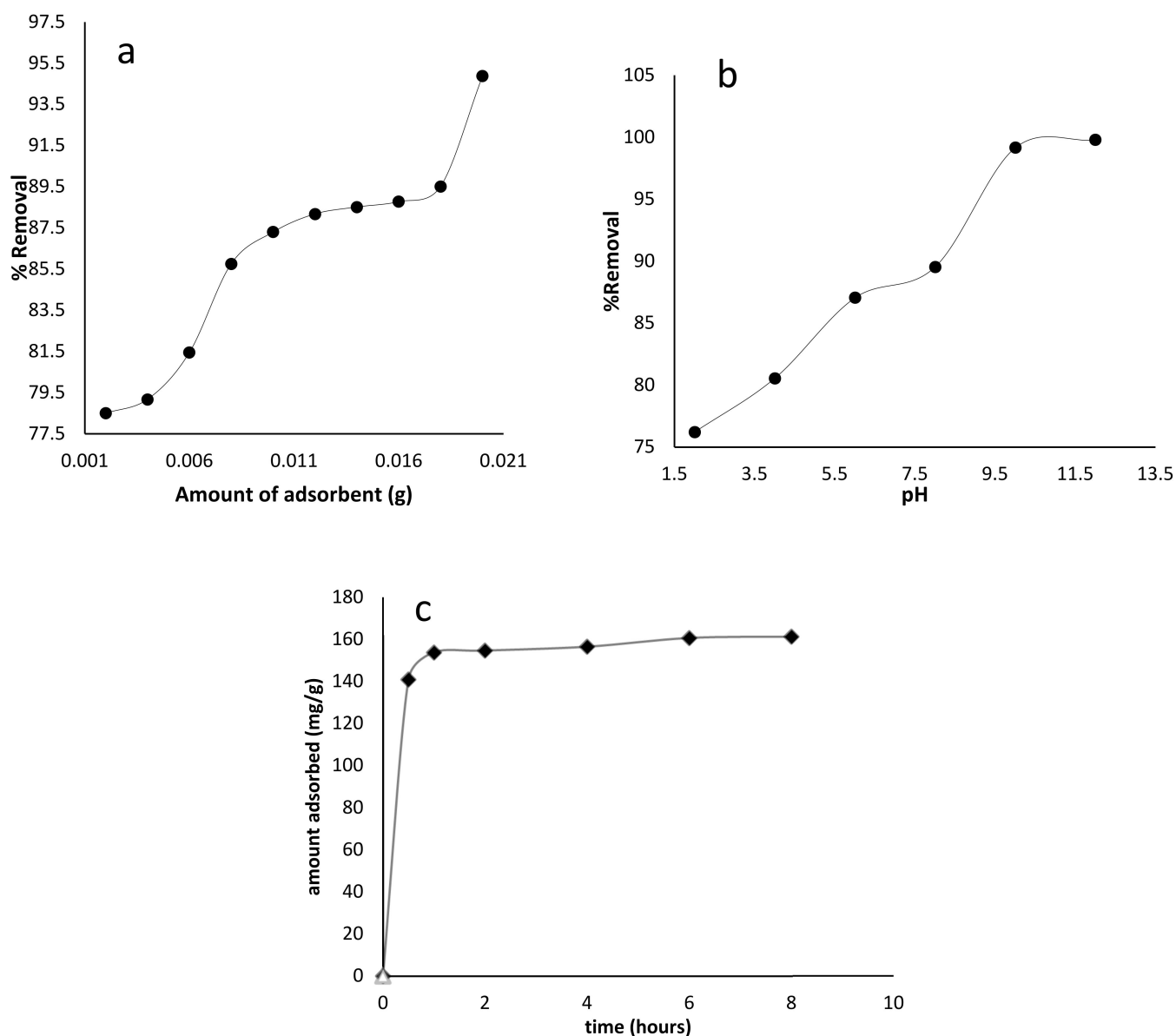


Figure 5. BB-3 adsorption on Pd-Ni/AC with the effects of (a) amount of adsorbent (b) pH and (c) contact time.

3.5. Adsorption Kinetics of BB-3 Adsorption

Adsorption kinetics must be considered for understanding the precise adsorption mechanism. Adsorption kinetics were applied for the assessment of adsorbate–adsorbent interaction and adsorption parameters [78]. Different kinetics models were applied to assess the kinetics of BB-3 adsorption on the prepared adsorbent.

The linear form of the pseudo-first-order kinetic equation can be given as follows [76,77]:

$$\log(q_e - q_t) = \log q_e - \frac{k_1}{2.303} t \quad (3)$$

In this equation, k_1 (min^{-1}) is the equilibrium rate constant, q_e and q_t are the amounts of dye adsorbed at equilibrium and t is time. The values of the constants k_1 and q_e were determined from the slope and intercept of the $\log(q_e - q_t)$ versus t [79] plot, which is shown in Figure 6a (Table 2).

The correlation coefficient R^2 was less than 0.9, which confirmed that this model did not show the best fit and proved that the sorption process was not a physisorption process.

The pseudo-second-order kinetic equation was expressed as [76,77]:

$$\frac{t}{q_t} = \frac{1}{k_2 q_e^2} + \frac{t}{q_e} \quad (4)$$

where k_2 (g/mg/min) is the pseudo-second-order rate constant. The slopes and intercepts of the plot of t/q_t versus t (Figure 6b) were used to calculate the q_e (mg/g) and k_2 values [80]. The pseudo-second-order constant k_2 (g/mg/min) and correlation coefficient R^2 values for the adsorption process of BB-3 on the Pd-Ni/AC were calculated and are listed in Table 2.

To understand the mechanism of the adsorption, an intraparticle diffusion model was used [76,77]:

$$q_t = k_{id} t_{\frac{1}{2}} + C \quad (5)$$

where k_{id} is the intraparticle diffusion constant, and C shows the thickness of boundary layer. The values are shown in Table 3. Figure 6c showed that the correlations do not pass through the origin, from which it can be concluded that the intraparticle and film diffusion are dominant.

The Elovich equation was applied to explain some aspects of the adsorption process. A mathematical form of the model can be expressed as [76,77]:

$$q_t = \ln \frac{\beta \alpha}{\alpha} + \frac{\ln t}{\beta} \quad (6)$$

where α is the initial sorption rate (mg/g/min), and the parameter β is related to the extent of surface coverage and activation energy for chemisorption (g/mg) [81–83]. The q_t vs. $\ln t$ was plotted and is shown in Figure 6d, and the value of α and β were determined, which are listed in Table 3.

The Natarajan and Khalaf equation gives the relationship between the initial dye concentration C_0 and the concentration at a certain time C_t [76,77]:

$$\log \left(\frac{C_0}{C_t} \right) = \frac{k}{2.303} t \quad (7)$$

where k is the Khalaf constant, its value calculated by plotting $\log \left(\frac{C_0}{C_t} \right)$ against time t (Figure 6e). The values of constants are given in Table 3.

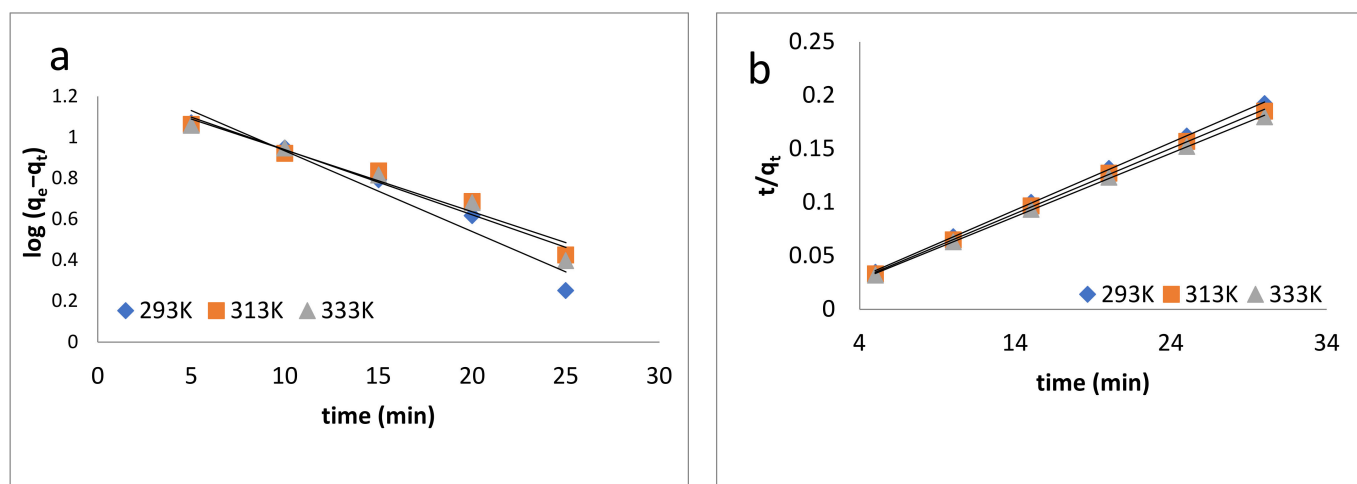


Figure 6. Cont.

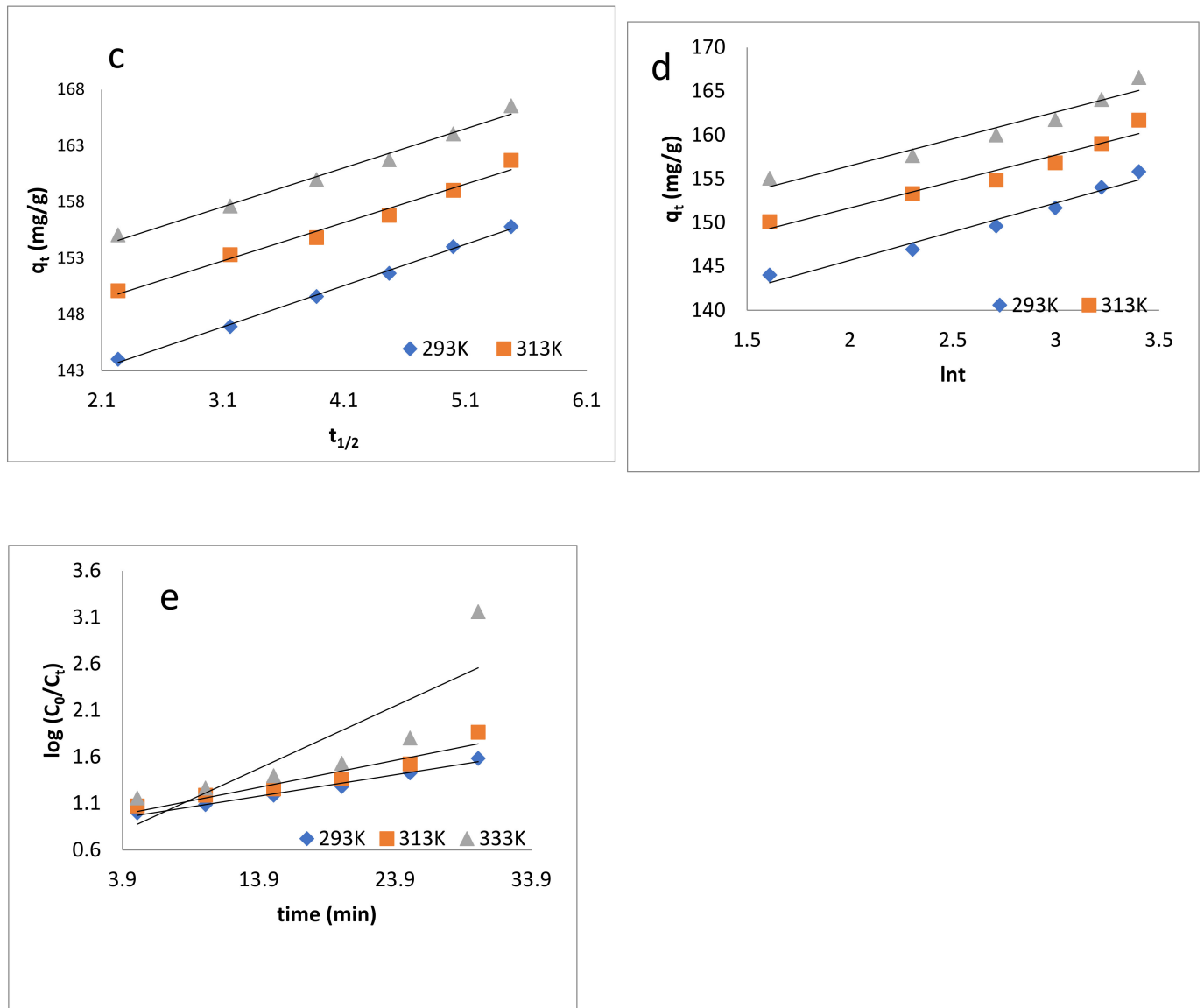


Figure 6. Kinetic models: (a) pseudo-first-order kinetics model; (b) pseudo-second-order kinetics model; (c) intraparticle diffusion model; (d) Elovich model; (e) Natarajan and Khalaf model.

Table 2. Temperature-dependent parameters of pseudo-first- and pseudo-second-order kinetics for adsorption of BB-3 on Pd–Ni/AC.

Parameter	293 K	313 K	333 K
Pseudo-first order			
q_e (cal) (mg/g)	21.281	17.414	17.782
q_e (exp) (mg/g)	155.825	161.705	166.55
k_1 (min^{-1})	0.091	0.069	0.073
$\Delta q\%$	86.3	89.6	89.3
R^2	0.948	0.960	0.960
Pseudo-second order			
q_e (cal) (mg/g)	158.73	163.93	169.49
q_e (exp) (mg/g)	155.825	161.705	166.551
K_2 (g/mg/min)	0.0086	0.0089	0.0087
$\Delta q\%$	1.85	1.39	1.76
R^2	0.999	0.999	0.999

Table 3. Parameters of other kinetic models for adsorption of BB-3 on Pd–Ni/AC.

Parameters	293 K	313 K	333 K
Intra-particle diffusion			
k_{id} (mg/g min ^{-1/2})	3.6702	3.4089	3.4618
C	135.53	142.21	146.87
R ²	0.9972	0.9808	0.986
Elovich equation			
α (mg/g min)	α (mg/g min)	α (mg/g min)	α (mg/g min)
β (mg/g min)	β (mg/g min)	β (mg/g min)	β (mg/g min)
R ²	R ²	R ²	R ²
Natarajan and Khalaf equation			
k (min ⁻¹)	k (min ⁻¹)	k (min ⁻¹)	k (min ⁻¹)
C	C	C	C

3.6. Isotherm Study

In order to identify the superficial properties and affinity of the adsorbent for adsorbate, isotherm models were used. The isotherm study signified how the adsorbate interacted with the adsorbent and helped in enumerating adsorption capacities. Langmuir, Freundlich and Temkin models were applied to explain the experimental data [84].

3.6.1. Langmuir Isotherm Model

This model can be successfully applied to the adsorption of different organic and inorganic pollutants on various adsorbents. According to this model, the adsorption occurs in monolayers, and the process takes place at certain homogenous sites contained by the adsorbent [76,77]. The model can be expressed as

$$\frac{C_e}{q_e} = \frac{C_e}{Q_m} + \frac{1}{K_L Q_m} \quad (8)$$

where C_e , q_e , K_L and Q_m are the concentration of dye at equilibrium (mg/L), amount adsorbed at equilibrium (mg/g), Langmuir constant (L/g), and maximum adsorption capacity (mg/g), respectively [85]. Plotting C_e/q_e , versus C_e enables us to determine the value of K_L and Q_m (from slope and intercept, Figure 7a–c). Their values, along with correlation coefficient R^2 , are given in Table 4. The Langmuir maximum adsorption capacities for sorption of BB-3 on Pd–Ni/AC were found to be 238.95, 277.78 and 333.3 mg/g at 293, 313 and 333 K, respectively. Langmuir isotherm provided high correlation coefficient values and fit well with the experimental data.

3.6.2. Freundlich Isotherm Model

This model concerns non ideal and reversible adsorption processes, which are not limited to the formation of monolayer [76,77]. This model can be expressed as

$$\ln q_e = \ln K_f + \frac{1}{n} \ln C_e \quad (9)$$

where C_e , q_e , K_f and $1/n$ are the equilibrium dye concentrations, amount of dye adsorbed at equilibrium, adsorption capacity at unit concentration and adsorption intensity, respectively.

When $1/n = 0$, the process will be irreversible; when $0 < 1/n < 1$, the process will be favorable and when $1/n > 1$, the process will be unfavorable [86].

A plot of $\ln q_e$ versus C_e enables us to determine the values of the above parameters from the slope and intercept (Figure 7d–f), the values of which are given in Table 4. The values of $1/n$ were: 0.3181, 0.3139 and 0.3379 at 293, 313 and 333 K, respectively, which indicates that the adsorption process was energetically favorable.

3.6.3. Temkin Isotherm Model

This model has two basic assumptions: (i) with the coverage of the surface, the heat of adsorption increases due to a positive interaction between adsorbate and adsorbent, and (ii) adsorption is described as a homogeneous distribution of binding sites of uniform energies up to a certain limit [76,77]. This model can be expressed as

$$q_e = B_1 \ln K_T + B_1 \ln C_e \tag{10}$$

where B_1 and K_T are the heat of adsorption and the equilibrium binding constant (L/mg) respectively [87]. Plotting q_e versus $\ln C_e$ enabled us to find out the values of these constants (Figure 7g–i). Their values are given in Table 4.

According to Table 4, the R^2 values show that the adsorption of BB-3 Pd–Ni/AC isotherm followed the Langmuir isotherm, as its value was greater than that of the Freundlich and Temkin isotherms. This indicates that the present adsorption processes can be better described by the Langmuir than the Freundlich and Temkin models, suggesting that adsorption occurs as the monolayer on the homogenous adsorbent surface.

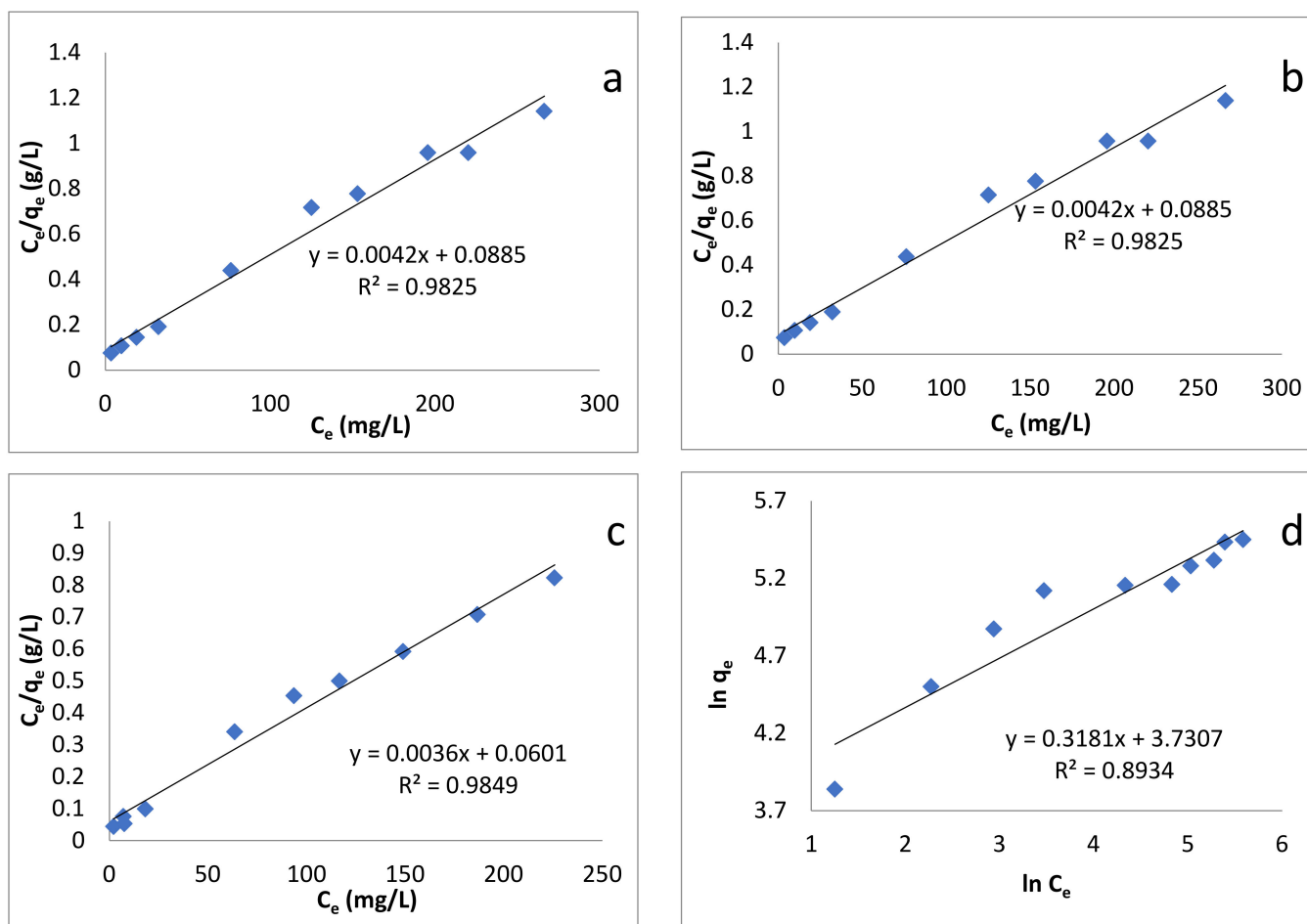


Figure 7. Cont.

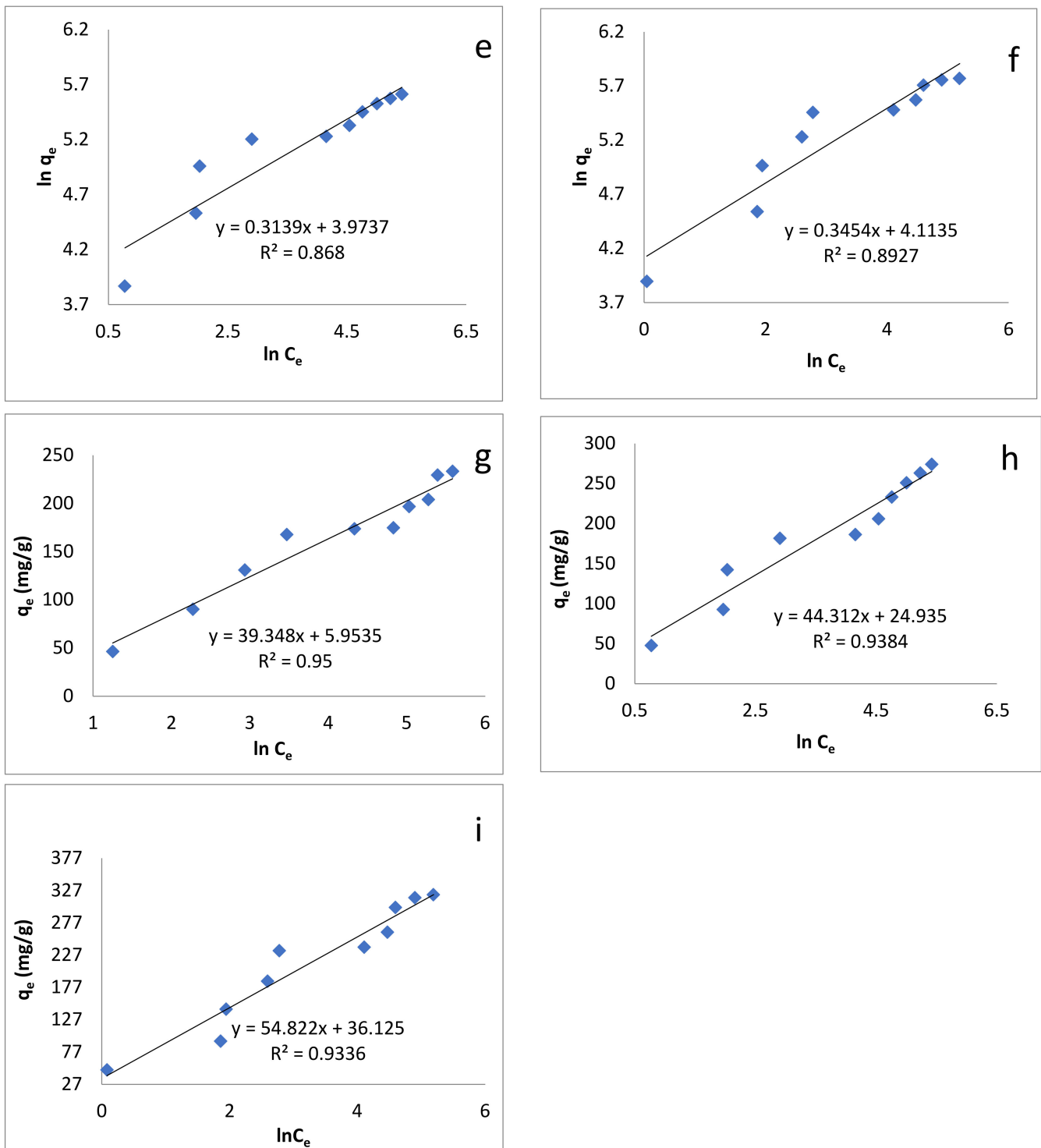


Figure 7. Adsorption isotherm models: (a) Langmuir isotherm at 293 K; (b) Langmuir isotherm at 313 K; (c) Langmuir isotherm at 333 K; (d) Freundlich isotherm at 293 K; (e) Freundlich isotherm at 313 K; (f) Freundlich isotherm at 333 K; (g) Temkin isotherm at 293 K; (h) Temkin isotherm at 313 K; (i) Temkin isotherm at 333 K.

Table 4. Parameters of isotherm study for adsorption of the BB-3 on Pd–Ni/AC.

Parameter	293 K	313 K	333 K
Langmuir isotherm model			
Q_m (mg/g)	238.95	277.78	333.3
K_a (g/mg)	0.00473	0.059	0.0824
R^2	0.9825	0.985	0.988
R_L	0.297	0.032	0.023
Freundlich isotherm model			
$1/n$	0.3181	0.3139	0.3379
K_f	41.591	53.088	62.95
R^2	0.8934	0.868	0.902
Temkin isotherm model			
B_1	39.348	44.312	52.997
K_T	1.163	1.717	2.264
R^2	0.95	0.9384	0.9297

3.7. Thermodynamic Study

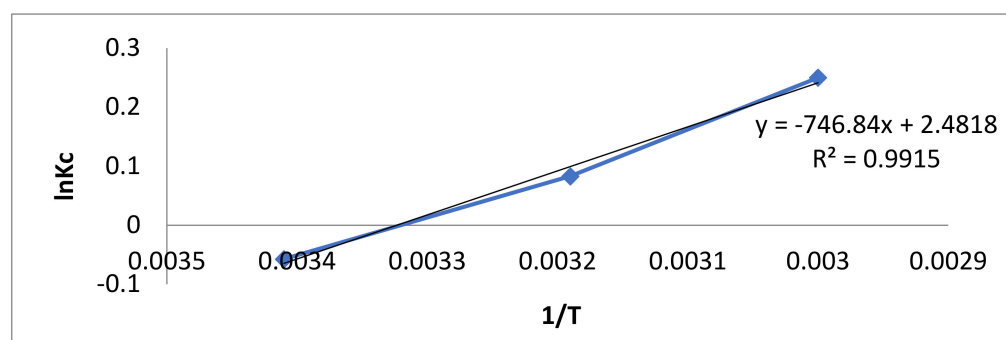
The thermodynamic parameters attained for the adsorption of BB-3 onto Pd–Ni/AC were calculated using the following equations [76,77]:

$$\Delta G^\circ = -RT \ln K_a \quad (11)$$

where $K_c = Q_e/C_e$.

$$\ln(K_c) = \frac{\Delta S^\circ}{R} - \frac{\Delta H^\circ}{RT} \quad (12)$$

ΔG° , ΔH° , ΔS° , K_c and K_a are the changes in Gibbs free energy, enthalpy, and entropy; the ratio of equilibrium adsorption; equilibrium concentration and the Langmuir constant, respectively. These values are given in Table 5, while the Van't Hoff plot is given in Figure 8.

**Figure 8.** Van't Hoff plot of BB-3 adsorption on ternary composite.

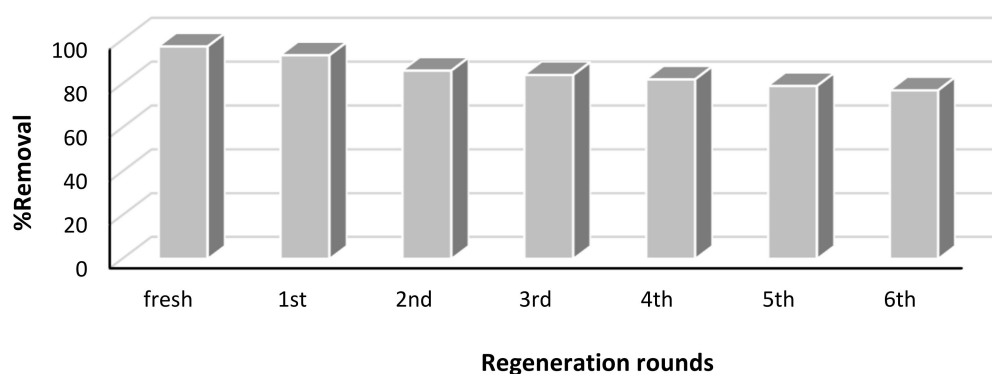
At different temperatures, the Gibbs free energy change (ΔG°) was found to be negative, indicating that the adsorption process was feasible and spontaneous. The decline in ΔG° values was found as temperature increased, indicating that the adsorption process occurs more favorably at lower temperatures [88]. The increased randomness at the dye/adsorbent interfaces and a strong affinity for the adsorption were verified by the positive value of change in enthalpy (ΔH°) [89]. During adsorption, a positive entropy change (ΔS°) indicated increased disorder at the solid–solution interface.

Table 5. Thermodynamic parameters for adsorption of BB-3 on Pd–Ni/AC.

	ΔG° (kJ/mol)		ΔH° (kJ/mol)	ΔS° (kJ/mol K)
293 K	313 K	333 K	−6.206	0.0242
−13.297	−13.780	−14.264		

3.8. Regeneration Study

To determine the regeneration efficiency of Pd–Ni/AC, the sample was washed with suitable eluents (dilute sodium hydroxide and ethanol) and then used several times, and the removal efficiency was monitored. From Figure 9 it was found that the removal efficiency was reduced up to 79% after six rounds of regeneration, showing that Pd–Ni/AC can be used with a sufficient efficiency up to several cycles.

**Figure 9.** Regeneration of adsorbents Pd–Ni/AC on dye treatment.

3.9. Comparing Adsorption Capacities of Reported Adsorbents with Current Adsorbent

Pd–Ni nanoparticles as an adsorbent showed maximum adsorption capacity compared with previously reported results [90–94] (Table 6). Hence, Pd–Ni nanoparticles may be an effective adsorbent for the removal of BB-3 dye and other pollutants. Previous studies have shown the assessment of the effects of pH and other factors on the solubility and performance of nanomaterials, which could be applied similarly in future studies [95–97].

Table 6. Comparison of adsorption capacities of various adsorbents for the removal of BB-3 within our current study.

Adsorbent	Pollutant	Q_{\max} (mg/g)	References
Ternary polymer composites	BB-3	200	[90]
Chitosan-based adsorbent	BB-3	134.5	[91]
Sulfuric Acid-Activated Montmorillonite Mineral	BB-3	277	[92]
durian peel (<i>Durio zibethinus</i> Murray)	BB-3	49.50	[93]
Weak acid acrylic resin	BB-3	59.53	[94]
Pd–Ni nanoparticles	BB-3	333	Current study

4. Conclusions

The aim of this study was to synthesize the Pd–Ni nanomaterials and to impregnate them onto activated carbon to enhance the surface of prepared nanoparticles. The prepared ternary adsorbent was used as an efficient adsorbent for the removal of basic blue 3 (BB-3) from water. The bifunctional alloy formation was confirmed from the metal analyses by XRD and the surface morphology by SEM analysis. About 94% removal of the BB-3 was achieved through the prepared adsorbent, indicating its high efficiency to remove the selected dye from water. Various equilibrium and kinetics models were used to calculate

different parameters of the adsorption, where pseudo-second-order kinetics and Langmuir models were found to be the best models that accommodated the experimental data with high R^2 values. The calculated thermodynamic parameters showed the process to be spontaneous ($\Delta S^\circ = 0.0242$ kJ/mol K and $\Delta G^\circ = -13.297$, -13.780 and -14.264 kJ/mol, respectively at 293, 313 and 333 K) and exothermic ($\Delta H^\circ = -6.206$ kJ/mol) in nature. The prepared adsorbent was effective in the removal of the selected dye and further tests are needed to evaluate its applicability for other pollutants as well.

Author Contributions: Conceptualization, M.Z.; methodology, A.U.; software, A.U.; validation, S.S.d.R., A.U. and I.Z.; formal analysis, A.U. and J.B.; investigation, A.U. and A.K. (Abbas Khan); resources, M.Z.; data curation, S.A.; writing—original draft preparation, I.Z.; writing—review and editing, M.S.K. and G.D.B.; visualization, R.K., M.S.K. and N.u.R.; supervision, M.Z.; project administration, M.Z., A.K. (Anna Kallistova), N.P. and M.M.G.; funding acquisition, M.Z. All authors have read and agreed to the published version of the manuscript.

Funding: This research was funded by project number T190087MIMV and the European Commission, MLTKT19481R “Identifying best available technologies for decentralized wastewater treatment and resource recovery for India” and SLTKT20427 “Sewage sludge treatment from heavy metals, emerging pollutants and recovery of metals by fungi”, and by projects KIK 15392 and 15401 by the European Commission.

Institutional Review Board Statement: Not applicable.

Informed Consent Statement: Not applicable.

Conflicts of Interest: The authors declare no conflict of interest. The funders had no role in the design of the study; in the collection, analyses or interpretation of data; in the writing of the manuscript or in the decision to publish the results.

References

- Anastopoulos, A.; Hosseini-Bandegharai, A.; Fu, J.; Mitropoulos, A.C.; Kyzas, G.Z. Use of Nanoparticles for Dye Adsorption. *J. Dispers. Sci. Technol.* **2018**, *39*, 836–847. [\[CrossRef\]](#)
- Marimuthu, A.J.; Antonisamy, S.; Malayandi, K.; Rajendran, P.-C.; Tsai, A.; Pugazhendhi, V.K.; Ponnusamy, S. Silver Nanoparticles in Dye Effluent Treatment: A Review on Synthesis, Treatment Methods, Mechanisms, Photocatalytic Degradation, Toxic Effects and Mitigation of Toxicity. *J. Photochem. Photobiol. B Biol.* **2020**, *205*, 111823. [\[CrossRef\]](#) [\[PubMed\]](#)
- Zeitoun, M.M.; Mehana, E. Impact of Water Pollution with Heavy Metals on Fish Health: Overview and Updates. *Glob. Vet.* **2014**, *12*, 219–231.
- Feng, P.; Zhang, H.-C.; Zhou, V.K.; Sharma, M. Water-Stable Metal-Organic Frameworks for Aqueous Removal of Heavy Metals and Radionuclides: A Review. *Chemosphere* **2018**, *209*, 783–800. [\[CrossRef\]](#)
- Eisenhauer, H.R. Oxidation of Phenolic Wastes. *J. Water Pollut. Control Fed.* **1964**, *36*, 1116–1128.
- Anju, A.P.; Ravi, S.; Bechan, S. Water Pollution with Special Reference to Pesticide Contamination in India. *J. Water Resour. Prot.* **2010**, *2010*. [\[CrossRef\]](#)
- Martínez, E.R.G.; Gonzalo, M.E.F.; Laespada, F.J.S.; San Roman, R.C. Evaluation of Surface-and Ground-Water Pollution due to Herbicides in Agricultural Areas of Zamora and Salamanca (Spain). *J. Chromatogr. A* **2000**, *869*, 471–480. [\[CrossRef\]](#)
- Cheng, D.; Ngo, H.H.; Guo, W.; Chang, S.W.; Nguyen, D.D.; Liu, Y.; Wei, Q.; Wei, D. A Critical Review on Antibiotics and Hormones in Swine Wastewater: Water Pollution Problems and Control Approaches. *J. Hazard. Mater.* **2020**, *387*, 121682. [\[CrossRef\]](#)
- Padhi, B. Pollution due to Synthetic Dyes Toxicity & Carcinogenicity Studies and Remediation. *Int. J. Environ. Sci.* **2012**, *3*, 940.
- Rehman, M.; Usman, T.H.; Bokhari, A.; Ul Haq, M.; Saeed, H.M.A.U.; Rahman, M.; Siddiq, A.; Rasheed, M.U.; Nisa, A. The Application of Cationic-Nonionic Mixed Micellar Media for Enhanced Solubilization of Direct Brown 2 Dye. *J. Mol. Liq.* **2020**, *301*, 112408. [\[CrossRef\]](#)
- Ikram, M.; Zahoor, M.; Gaber El-Saber, B. Biodegradation and decolorization of textile dyes by bacterial strains: A biological approach for wastewater treatment. *Z. Phys. Chem.* **2020**. [\[CrossRef\]](#)
- Gupta, V.K.; Kumar, R.; Nayak, A.; Saleh, T.A.; Barakat, M.A. Adsorptive Removal of Dyes from Aqueous Solution onto Carbon Nanotubes: A Review. *Adv. Colloid Interface Sci.* **2013**, *193–194*, 24–34. [\[CrossRef\]](#)
- Tara, S.I.; Siddiqui, G.; Rathi, S.A.; Chaudhry, A.M.; Asiri, N. Nano-Engineered Adsorbent for the Removal of Dyes from Water: A Review. *Curr. Anal. Chem.* **2020**, *16*, 14–40. [\[CrossRef\]](#)
- Routoula, S.V.; Patwardhan, E. Degradation of Anthraquinone Dyes from Effluents: A Review Focusing on Enzymatic Dye Degradation with Industrial Potential. *Environ. Sci. Technol.* **2020**, *54*, 647–664. [\[CrossRef\]](#)

15. Allen, S.; McKay, G.; Porter, J.F. Adsorption Isotherm Models for Basic Dye Adsorption by Peat in Single and Binary Component Systems. *J. Colloid Interface Sci.* **2004**, *280*, 322–333. [[CrossRef](#)]
16. Arica, M.Y.; Bayramoğlu, G. Biosorption of Reactive Red-120 dye from Aqueous Solution by Native and Modified Fungus Biomass Preparations of *Lentinus Sajor-caju*. *J. Hazard. Mater.* **2007**, *149*, 499–507. [[CrossRef](#)]
17. Osugi, M.E.; Umbuzeiro, G.A.; De Castro, F.J.; Zaroni, M.V.B. Photoelectrocatalytic Oxidation of Remazol Turquoise Blue and Toxicological Assessment of its Oxidation Products. *J. Hazard. Mater.* **2006**, *137*, 871–877. [[CrossRef](#)]
18. Bafana, A.; Jain, M.; Agrawal, G.; Chakrabarti, T. Bacterial Reduction in Genotoxicity of Direct Red 28 Dye. *Chemosphere* **2009**, *74*, 1404–1406. [[CrossRef](#)]
19. Wong, P.; Yuen, P. Decolorization and Biodegradation of Methyl Red by *Klebsiella Pneumoniae* RS-13. *Water Res.* **1996**, *30*, 1736–1744. [[CrossRef](#)]
20. Fiedurek, J.; Gromada, A. Production of Catalase and Glucose Oxidase by *Aspergillus Niger* using Unconventional Oxygenation of Culture. *J. Appl. Microbiol.* **2000**, *89*, 85–89. [[CrossRef](#)]
21. Nigam, P.; Armour, G.; Banat, I.; Singh, D.; Marchant, R. Physical Removal of Textile Dyes from Effluents and Solid-State Fermentation of Dye-Adsorbed Agricultural Residues. *Bioresour. Technol.* **2000**, *72*, 219–226. [[CrossRef](#)]
22. Bayramoğlu, G.; Arica, M.Y. Biosorption of Benzidine based Textile Dyes. Direct Blue 1 and Direct Red 128" using Native and Heat-Treated Biomass of *Trametes Versicolor*. *J. Hazard. Mater.* **2007**, *143*, 135–143. [[CrossRef](#)]
23. Gadd, G.M. Metals and Microorganisms: A Problem of Definition. *FEMS Microbiol. Lett.* **1992**, *100*, 197–203. [[CrossRef](#)]
24. Binupriya, A.; Sathishkumar, M.; Swaminathan, K.; Kuz, C.; Yun, S. Comparative Studies on Removal of Congo Red by Native and Modified Mycelial Pellets of *Trametes Versicolor* in Various Reactor Modes. *Bioresour. Technol.* **2008**, *99*, 1080–1088. [[CrossRef](#)] [[PubMed](#)]
25. Nigam, P.S.N.; Banat, I.; Oxspring, D.; Marchant, R.; Singh, D.; Smyth, W. A New Facultative Anaerobic Filamentous Fungus Capable of Growth on Recalcitrant Textile Dyes as Sole Carbon Source. *Microbios* **1995**, *84*, 171–185.
26. Ponraj, M.; Gokila, K.; Zambare, V. Bacterial Decolorization of Textile Dye-Orange 3R. *Int. J. Adv. Biotechnol. Res.* **2011**, *2*, 168–177.
27. Tapia-Tussell, R.; Pereira-Patrón, A.; Alzate-Gaviria, L.; Lizama-Uc, G.; Pérez-Brito, D.; Solis-Pereira, S. Decolorization of Textile Effluent by *Trametes Hirsuta* Bm-2 and lac-T as Possible Main Laccase-Contributing Gene. *Curr. Microbiol.* **2020**, *77*, 3953–3961. [[CrossRef](#)]
28. Ekanayake, M.S.; Udayanga, D.; Wijesekara, I.; Manage, P. Phytoremediation of Synthetic Textile Dyes: Biosorption and Enzymatic Degradation Involved in Efficient Dye Decolorization by *Eichhornia Crassipes* (Mart.) Solms and *Pistia Stratiotes* L. *Environ. Sci. Pollut. Res.* **2021**, 1–11. [[CrossRef](#)]
29. Dellamatrice, P.M.; Silva-Stenico, M.E.; Moraes, L.A.B.D.; Fiore, M.F.; Monteiro, T.R. Degradation of Textile Dyes by Cyanobacteria. *Braz. J. Microbiol.* **2017**, *48*, 25–31. [[CrossRef](#)]
30. Lopez-Barbosa, N.; Florez, S.L.; Cruz, J.C.; Ornelas-Soto, N.; Osmá, J.F. Congo Red Decolorization Using Textile Filters and Laccase-Based Nanocomposites in Continuous Flow Bioreactors. *Nanomaterials* **2020**, *10*, 1227. [[CrossRef](#)]
31. Nagajyothi, P.; Prabhakar Vattikuti, S.; Devarayapalli, K.; Yoo, K.; Shim, J.; Sreekanth, T. Green Synthesis: Photocatalytic Degradation of Textile Dyes using Metal and Metal Oxide Nanoparticles-Latest Trends and Advancements. *Crit. Rev. Environ. Sci. Technol.* **2020**, *50*, 2617–2723. [[CrossRef](#)]
32. Bilińska, L.; Blus, K.; Foszpańczyk, M.; Gmurek, M.; Ledakowicz, S. Catalytic Ozonation of Textile Wastewater as a Polishing Step after Industrial Scale Electrocoagulation. *J. Environ. Manag.* **2020**, *265*, 110502. [[CrossRef](#)] [[PubMed](#)]
33. Han, Y.; Li, H.; Liu, M.; Sang, Y.; Liang, C.; Chen, J. Purification Treatment of Dyes Wastewater with a Novel Micro-Electrolysis Reactor. *Sep. Purif. Technol.* **2016**, *170*, 241–247. [[CrossRef](#)]
34. Wawrzkiwicz, M.; Hubicki, Z. Anion Exchange Resins as Effective Sorbents for Removal of Acid, Reactive, and Direct Dyes from Textile Wastewaters. *Ion Exch. Stud. Appl.* **2015**, 37–72. [[CrossRef](#)]
35. Alderete, B.L.; da Silva, J.; Godoi, R.; da Silva, F.R.; Taffarel, S.R.; da Silva, L.P.; Garcia, A.L.H.; Júnior, H.M.; de Amorim, H.L.N.; Picada, J.N. Evaluation of Toxicity and Mutagenicity of a Synthetic Effluent Containing Azo Dye after Advanced Oxidation Process Treatment. *Chemosphere* **2020**, *263*, 128291. [[CrossRef](#)]
36. Long, Q.; Zhang, Z.; Qi, G.; Wang, Z.; Chen, Y.; Liu, Z.-Q. Fabrication of Chitosan Nanofiltration Membranes by the Film Casting Strategy for Effective Removal of Dyes/Salts in Textile Wastewater. *ACS Sustain. Chem. Eng.* **2020**, *8*, 2512–2522. [[CrossRef](#)]
37. Demissie, H.; An, G.; Jiao, R.; Ritigala, T.; Lu, S.; Wang, D. Modification of High Content Nanocluster-Based Coagulation for Rapid Removal of Dye from Water and the Mechanism. *Sep. Purif. Technol.* **2021**, *259*, 117845. [[CrossRef](#)]
38. Wang, K.; Wei, T.; Li, Y.; He, L.; Lv, Y.; Chen, L.; Ahmad, A.; Xu, Y.; Shi, Y. Flocculation-to-Adsorption Transition of Novel Salt-Responsive Polyelectrolyte for Recycling of Highly Polluted Saline Textile Effluents. *Chem. Eng. J.* **2021**, *413*, 127410. [[CrossRef](#)]
39. Pakhale, V.D.; Gogate, P.R. Removal of Rhodamine 6G from Industrial Wastewater Using Combination Approach of Adsorption Followed by Sonication. *Arab. J. Sci. Eng.* **2021**, 1–12. [[CrossRef](#)]
40. Aljeboree, A.M.; Al-Gubury, H.Y.; Bader, A.T.; Alkaim, A.F. Adsorption of Textile Dyes in the Presence Either Clay or Activated Carbon as a Technological Models: A Review. *J. Crit. Rev.* **2020**, *7*, 620–626.
41. Deniz, F. Adsorption Properties of Low-Cost Biomaterial Derived from *Prunus Amygdalus* L. for Dye Removal from Water. *Sci. World J.* **2013**, 2013. [[CrossRef](#)]

42. Rafatullah, M.; Sulaiman, O.; Hashim, R.; Ahmad, A. Adsorption of Methylene Blue on Low-Cost Adsorbents: A Review. *J. Hazard. Mater.* **2010**, *177*, 70–80. [[CrossRef](#)]
43. Dąbrowski, A. Adsorption—From Theory to Practice. *Adv. Colloid Interface Sci.* **2001**, *93*, 135–224. [[CrossRef](#)]
44. Allen, S.; Koumanova, B. Decolourisation of Water/Wastewater using Adsorption. *J. Univ. Chem. Technol. Metall.* **2005**, *40*, 175–192.
45. Adak, A.; Bandyopadhyay, M.; Pal, A. Adsorption of Anionic Surfactant on Alumina and Reuse of the Surfactant-Modified Alumina for the Removal of Crystal Violet from Aquatic Environment. *J. Environ. Sci. Health* **2005**, *40*, 167–182. [[CrossRef](#)]
46. Kausar, A.; Iqbal, M.; Javed, A.; Aftab, K.; Bhatti, H.N.; Nouren, S. Dyes Adsorption using Clay and Modified Clay: A Review. *J. Mol. Liq.* **2018**, *256*, 395–407. [[CrossRef](#)]
47. Kumar, P.S.; Joshiba, G.J.; Femina, C.C.; Varshini, P.; Priyadharshini, S.; Karthick, M.A.; Jothirani, R. A Critical Review on Recent Developments in the Low-Cost Adsorption of Dyes from Wastewater. *Desalin. Water Treat.* **2019**, *172*, 395–416. [[CrossRef](#)]
48. Mouni, L.; Belkhir, L.; Bollinger, J.-C.; Bouzaza, A.; Assadi, A.; Tirri, A.; Dahmoune, F.; Madani, K.; Remini, H. Removal of Methylene Blue from Aqueous Solutions by Adsorption on Kaolin: Kinetic and Equilibrium Studies. *Appl. Clay Sci.* **2018**, *153*, 38–45. [[CrossRef](#)]
49. Huang, Z.; Li, Y.; Chen, W.; Shi, J.; Zhang, N.; Wang, X.; Li, Z.; Gao, L.; Zhang, Y. Modified Bentonite Adsorption of Organic Pollutants of Dye Wastewater. *Mater. Chem. Phys.* **2017**, *202*, 266–276. [[CrossRef](#)]
50. Astuti, W.; Sulistyarningsih, T.; Maksiola, M. Equilibrium and Kinetics of Adsorption of Methyl Violet from Aqueous Solutions Using Modified Ceiba Pentandra Sawdust. *Asian J. Chem.* **2017**, *29*, 133–138. [[CrossRef](#)]
51. Alouani, M.; Alehyen, S.; Achouri, M.; Taibi, M. Removal of Cationic Dye—Methylene Blue—From Aqueous Solution by Adsorption on Fly Ash—Based Geopolymer. *J. Mater. Environ. Sci.* **2018**, *9*, 32–46.
52. Brião, G.V.; Jahn, S.L.; Foletto, E.L.; Dotto, G.L. Highly Efficient and Reusable Mesoporous Zeolite Synthesized from a Biopolymer for Cationic Dyes Adsorption. *Colloids Surf. A Physicochem. Eng. Asp.* **2018**, *556*, 43–50. [[CrossRef](#)]
53. Yao, S.; Xu, T.; Zhao, N.; Zhang, L.; Huo, Q.; Liu, Y. An Anionic Metal–Organic Framework with Ternary Building Units for Rapid and Selective Adsorption of Dyes. *Dalton Trans.* **2017**, *46*, 3332–3337. [[CrossRef](#)] [[PubMed](#)]
54. Nakhjiri, M.T.; Marandi, G.B.; Kurdtabar, M. Poly (AA-co-VPA) Hydrogel Cross-Linked with N-Maleyl Chitosan as Dye Adsorbent: Isotherms, Kinetics and Thermodynamic Investigation. *Int. J. Biol. Macromol.* **2018**, *117*, 152–166. [[CrossRef](#)]
55. Kyzas, G.Z.; Bikiaris, D.N.; Lazaridis, N.K. Selective Separation of Basic and Reactive Dyes by Molecularly Imprinted Polymers (MIPs). *Chem. Eng. J.* **2009**, *149*, 263–272. [[CrossRef](#)]
56. Deb, A.; Kanmani, M.; Debnath, A.; Bhowmik, K.L.; Saha, B. Ultrasonic Assisted Enhanced Adsorption of Methyl Orange Dye onto Polyaniline Impregnated Zinc Oxide Nanoparticles: Kinetic, Isotherm and Optimization of Process Parameters. *Ultrason. Sonochem.* **2019**, *54*, 290–301. [[CrossRef](#)]
57. Gu, J.; Hu, C.; Zhang, W.; Dichiaro, A.B. Reagentless Preparation of Shape Memory Cellulose Nanofibril Aerogels Decorated with Pd Nanoparticles and their Application in Dye Discoloration. *Appl. Catal. B Environ.* **2018**, *237*, 482–490. [[CrossRef](#)]
58. Mirzajani, R.; Karimi, S. Ultrasonic Assisted Synthesis of Magnetic Ni-Ag Bimetallic Nanoparticles Supported on Reduced Graphene Oxide for Sonochemical Simultaneous Removal of Sunset Yellow and Tartrazine Dyes by Response Surface Optimization: Application of Derivative Spectrophotometry. *Ultrason. Sonochem.* **2019**, *50*, 239–250.
59. Hasan, S. A Review on Nanoparticles: Their Synthesis and Types. *Res. J. Recent Sci.* **2015**, *2277*, 2502.
60. Wiechers, J.W.; Musee, N. Engineered Inorganic Nanoparticles and Cosmetics: Facts, Issues, Knowledge Gaps and Challenges. *J. Biomed. Nanotechnol.* **2010**, *6*, 408–431. [[CrossRef](#)]
61. Teng, W.-Y.; Jeng, S.-C.; Kuo, C.-W.; Lin, Y.-R.; Liao, C.-C.; Chin, W.-K. Nanoparticles-Doped Guest-Host Liquid Crystal Displays. *Opt. Lett.* **2008**, *33*, 1663–1665. [[CrossRef](#)]
62. Li, Y.; Hong, X.M.; Collard, D.M.; El-Sayed, M.A. Suzuki Cross-Coupling Reactions Catalyzed by Palladium Nanoparticles in Aqueous Solution. *Organ. Lett.* **2000**, *2*, 2385–2388. [[CrossRef](#)]
63. Chavanpatil, M.D.; Khdair, A.; Panyam, J. Surfactant-Polymer Nanoparticles: A Novel Platform for Sustained and Enhanced Cellular Delivery of Water-Soluble Molecules. *Pharm. Res.* **2007**, *24*, 803–810. [[CrossRef](#)]
64. Roy, I.; Ohulchanskyy, T.Y.; Pudavar, H.E.; Bergey, E.J.; Oseroff, A.R.; Morgan, J.; Dougherty, T.J.; Prasad, P.N. Ceramic-based Nanoparticles Entrapping Water-Insoluble Photosensitizing Anticancer Drugs: A NOVEL drug–Carrier System for Photodynamic Therapy. *J. Am. Chem. Soc.* **2003**, *125*, 7860–7865. [[CrossRef](#)]
65. Jia, Q.; Nguyen, P.K.; Gu, Z.; Zhang, X.; Liu, M.; Tian, X.; Ma, L.; Gong, L.; Mu, X.; Chang, Y. N-Doped Bismuth Molybdate Decorated with Pt Nanoparticles Removal Azo Dyes Efficiently via the Synergistic Effect of Adsorption and Photocatalysis. *J. Alloys Compd.* **2021**, *863*, 158336. [[CrossRef](#)]
66. Lim, I.I.S.; Goroleski, F.; Mott, D.; Kariuki, N.; Ip, W.; Luo, J.; Zhong, C.-J. Adsorption of Cyanine Dyes on Gold Nanoparticles and Formation of J-Aggregates in the Nanoparticle Assembly. *J. Phys. Chem. B* **2006**, *110*, 6673–6682. [[CrossRef](#)]
67. Asfaram, A.; Ghaedi, M.; Agarwal, S.; Tyagi, I.; Gupta, V.K. Removal of Basic Dye Auramine-O by ZnS: Cu Nanoparticles Loaded on Activated Carbon: Optimization of Parameters using Response Surface Methodology with Central Composite Design. *RSC Adv.* **2015**, *5*, 18438–18450. [[CrossRef](#)]
68. Bokare, A.D.; Chikate, R.C.; Rode, C.V.; Paknikar, K.M. Iron-Nickel Bimetallic Nanoparticles for Reductive Degradation of Azo Dye Orange G in Aqueous Solution. *Appl. Catal. B Environ.* **2008**, *79*, 270–278. [[CrossRef](#)]

69. Ismail, M.; Khan, M.; Khan, S.B.; Khan, M.A.; Akhtar, K.; Asiri, A.M. Green Synthesis of Plant Supported CuAg and CuNi Bimetallic Nanoparticles in the Reduction of Nitrophenols and Organic Dyes for Water Treatment. *J. Mol. Liq.* **2018**, *260*, 78–91. [[CrossRef](#)]
70. Gautam, R.K.; Rawat, V.; Banerjee, S.; Sanroman, M.A.; Soni, S.; Singh, S.K.; Chattopadhyaya, M.C. Synthesis of Bimetallic Fe–Zn Nanoparticles and its Application towards Adsorptive Removal of Carcinogenic Dye Malachite Green and Congo Red in Water. *J. Mol. Liq.* **2015**, *212*, 227–236. [[CrossRef](#)]
71. Kaewmanee, T.; Phuruangrat, A.; Thongtem, T.; Thongtem, S. Solvothermal Synthesis of Mn–Zn Ferrite (core)@ SiO₂ (shell)/BiOBr_{0.5}Cl_{0.5} Nanocomposites used for Adsorption and Photocatalysis Combination. *Ceram. Int.* **2020**, *46*, 3655–3662. [[CrossRef](#)]
72. Xu, J.; Liu, X.; Lowry, G.V.; Cao, Z.; Zhao, H.; Zhou, J.L.; Xu, X. Dechlorination Mechanism of 2, 4-Dichlorophenol by Magnetic MWCNTs Supported Pd/Fe Nanohybrids: Rapid Adsorption, Gradual Dechlorination, and Desorption of Phenol. *ACS Appl. Mater. Interfaces* **2016**, *8*, 7333–7342. [[CrossRef](#)] [[PubMed](#)]
73. Sharma, G.; Gupta, V.K.; Agarwal, S.; Kumar, A.; Thakur, S.; Pathania, D. Fabrication and Characterization of Fe@ MoPO Nanoparticles: Ion Exchange Behavior and Photocatalytic Activity against Malachite Green. *J. Mol. Liq.* **2016**, *219*, 1137–1143. [[CrossRef](#)]
74. Sharma, G.; Kumar, A.; Sharma, S.; Naushad, M.; Dwivedi, R.P.; AlOthman, Z.A.; Mola, G.T. Novel Development of Nanoparticles to Bimetallic Nanoparticles and Their Composites: A Review. *J. King Saud Univ. Sci.* **2019**, *31*, 257–269. [[CrossRef](#)]
75. Alvarenga, G.M.; Gallo, I.B.C.; Villullas, H.M. Enhancement of Ethanol Oxidation on Pd Nanoparticles Supported on Carbon-Antimony tin Oxide Hybrids Unveils the Relevance of Electronic Effects. *J. Catal.* **2017**, *348*, 1–8. [[CrossRef](#)]
76. Shamim, A.; Begum, A.H.M.; Hyder, G.; Vahdat, N. Adsorption Isotherm and Kinetic Studies of As(V) Removal from Aqueous Solution Using Cattle Bone Char. *J. Water Supply Res. Technol. AQUA* **2016**, *65*, 244–252.
77. Hyder, M.G.; Shamim, A.B.; Nosa, O.; Egiebor, A.H. Sorption Studies of Cr(VI) from Aqueous Solution using Biochar as an Adsorbent. *Water Sci. Technol.* **2014**, *69*, 2265–2271. [[CrossRef](#)]
78. Ghaedi, A.M.; Ansari, M.H.; Asghari, A. Removal of Malachite Green from Aqueous Solution by Zinc Oxide Nanoparticle Loaded on Activated Carbon: Kinetics and Isotherm Study. *J. Ind. Eng. Chem.* **2014**, *20*, 17–28. [[CrossRef](#)]
79. Ghaedi, M.; Ansari, A.; Sahraei, R. ZnS: Cu Nanoparticles Loaded on Activated Carbon as Novel Adsorbent for Kinetic, Thermodynamic and Isotherm Studies of Reactive Orange 12 and Direct Yellow 12 Adsorption. *Spectrochim. Acta Part A Mol. Biomol. Spectrosc.* **2013**, *114*, 687–694. [[CrossRef](#)]
80. Asfaram, A.; Ghaedi, M.; Hajati, S.; Rezaeinejad, M.; Goudarzi, A.; Purkait, M.K. Rapid Removal of Auramine-O and Methylene Blue by ZnS: Cu Nanoparticles Loaded on Activated Carbon: A Response Surface Methodology Approach. *J. Taiwan Inst. Chem. Eng.* **2015**, *53*, 80–91. [[CrossRef](#)]
81. Özacar, M.; Şengil, İ.A. Application of Kinetic Models to the Sorption of Disperse Dyes onto Alunite. *Colloids Surf. A Physicochem. Eng. Asp.* **2004**, *242*, 105–113. [[CrossRef](#)]
82. Girish, C.; Murty, V.R. Mass Transfer Studies on Adsorption of Phenol from Wastewater using Lantana Camara, Forest Waste. *Int. J. Chem. Eng.* **2016**, *2016*. [[CrossRef](#)]
83. Okoye, A.; Ejikeme, P.; Onukwuli, O. Lead Removal from Wastewater using Fluted Pumpkin Seed Shell Activated Carbon: Adsorption Modeling and Kinetics. *Int. J. Environ. Sci. Technol.* **2010**, *7*, 793–800. [[CrossRef](#)]
84. Saxena, M.; Sharma, N.; Saxena, R. Highly Efficient and Rapid Removal of a Toxic Dye: Adsorption Kinetics, Isotherm, and Mechanism Studies on Functionalized Multiwalled Carbon Nanotubes. *Surf. Interfaces* **2020**, *21*, 100639. [[CrossRef](#)]
85. Langmuir, I. The Adsorption of Gases on Plane Surfaces of Glass, Mica and Platinum. *J. Am. Chem. Soc.* **1918**, *40*, 1361–1403. [[CrossRef](#)]
86. Freundlich, H. Over the Adsorption in Solution. *J. Phys. Chem.* **1906**, *57*, 1100–1107.
87. Munagapati, V.S.; Kim, D.-S. Equilibrium Isotherms, Kinetics, and Thermodynamics Studies for Congo Red Adsorption using Calcium Alginate Beads Impregnated with Nano-Goethite. *Ecotoxicol. Environ. Saf.* **2017**, *141*, 226–234. [[CrossRef](#)]
88. Namasivayam, C.; Senthilkumar, S. Recycling of Industrial Solid Waste for the Removal of Mercury (II) by Adsorption Process. *Chemosphere* **1997**, *34*, 357–375. [[CrossRef](#)]
89. Aljeboree, A.M.; Baqir, S.J.; Alkaim, A.F. Experimental Studies of Thermodynamics Parameters: As a Model Adsorption and Removal of TEXTILE. *J. Phys. Conf. Ser.* **2020**, 012099. [[CrossRef](#)]
90. Karakuş, S.; Şişmanoğlu, S.; Akdut, G.; Ürk, Ö.; Şişmanoğlu, E.T.T.; Kilislioğlu, A. Removal of Basic Blue 3 from the Aqueous Solution with Ternary Polymer Nanocomposite: Swelling, Kinetics, Isotherms and Error Function. *J. Chem. Soc. Pak.* **2017**, *39*, 17–25.
91. Crini, G.E.; Gimbert, F.; Robert, C.; Martel, B.; Adama, O.; Morin-Crini, N.; De Giorgi, F.; Badot, P.-M. The Removal of Basic Blue 3 from Aqueous Solutions by Chitosan-Based Adsorbent: Batch Studies. *J. Hazard. Mater.* **2008**, *153*, 96–106. [[CrossRef](#)] [[PubMed](#)]
92. Taşar, Ş.; Kaya, F.; Özer, A. Adsorption of CI Basic Blue 3 Dye Molecules from Aqueous Media by Sulfuric Acid-Activated Montmorillonite Mineral. *J. Turk. Chem. Soc. Chem. Eng.* **2017**, *1*, 1–16.
93. Ong, S.-T.; Tan, S.-Y.; Khoo, E.-C.; Lee, S.-L.; Ha, S.-T. Equilibrium Studies for Basic Blue 3 Adsorption onto Durian Peel (*Durio Zibethinus Murray*). *Desalin. Water Treat.* **2012**, *45*, 161–169. [[CrossRef](#)]
94. Bârsănescu, A.; Buhăceanu, R.; Dulman, V. Removal of Basic Blue 3 by Sorption onto a Weak Acid Acrylic Resin. *J. Appl. Polym. Sci.* **2009**, *113*, 607–614. [[CrossRef](#)]

-
95. Tenno, T.; Rikmann, E.; Zekker, I.; Tenno, T. Modelling the Solubility of Sparingly Soluble Compounds Depending on Their Particles Size. *Proc. Est. Acad. Sci.* **2018**, *67*, 300–302. [[CrossRef](#)]
 96. Zekker, I.; Tenno, T.; Selberg, A.; Uiga, K. Dissolution Modeling and Experimental Measurement of CaS-H₂O Binary System. *Chin. J. Chem.* **2011**, *29*, 2327–2336. [[CrossRef](#)]
 97. Tenno, T.; Rikmann, E.; Uiga, K.; Zekker, I.; Mashirin, A.; Tenno, T. A Novel Proton Transfer Model of the Closed Equilibrium System H₂O–CO₂–CaCO₃–NH_x. *Proc. Est. Acad. Sci.* **2018**, *4017*, 2. [[CrossRef](#)]